



Contents lists available at ScienceDirect

Arabian Journal of Chemistry

journal homepage: www.ksu.edu.sa

Original article

Fabrication of lanthanum-silane film by electrochemically assisted sol-gel method for enhanced corrosion resistance of sintered NdFeB

Zhu Tao^a, Li Jiang^{a,*}, Wentao Ju^a, Yanxia Liang^a, Yumeng Yang^a, Guoying Wei^a, Yu Chen^b, Zhao Zhang^c^a College of Materials and Chemistry, China Jiliang University, Hangzhou, Zhejiang 310018, China^b School of Materials and Energy, Foshan University, Foshan, Guangdong 528000, China^c Department of Chemistry, Zhejiang University, Hangzhou, Zhejiang 310027, China

ARTICLE INFO

Keywords:

Sintered NdFeB
Lanthanum-silane film
Corrosion resistance
Magnetism

ABSTRACT

The surface of sintered NdFeB was coated with a lanthanum-silane film using an electrochemically assisted sol-gel method to improve its protective performance. The electrochemically assisted deposition mechanism is localized alkali catalysis at the surface with an applied cathodic potential, which promotes the condensation reaction of hydrolyzed silanol groups on the sintered NdFeB substrate surface and the production of lanthanum oxide/hydroxide in the silane film as well. Contact angle test results indicated that the hydrophobicity of the lanthanum-silane film was considerably enhanced compared to the bare sintered NdFeB substrate, and the water contact angle was above 150°. Meanwhile, electrochemical measurements suggested that the lanthanum-doped silane film significantly reduced the corrosion rate of the sintered NdFeB magnet in a 3.5 wt% NaCl solution with an I_{corr} value of $5.26 \times 10^{-7} \text{ A cm}^{-2}$, and the protection efficiency reached 92.5%. Furthermore, the magnetic properties of the lanthanum-silane film-coated sintered NdFeB sample were also evaluated and the effect was negligible.

1. Introduction

Sintered NdFeB permanent magnets have been widely used in communication, audio, new energy vehicles, and other fields, due to their notable attributes such as high remanence, high coercivity, and maximum magnetic energy product (Song et al., 2019; Sheridan et al., 2014). However, the multiphase structure and potential difference between different phases render sintered NdFeB magnets highly susceptible to electrochemical corrosion, resulting in a shortened service life and constrained development potential (Wu et al., 2021). Consequently, there is a significant research focus on enhancing the corrosion resistance of sintered NdFeB magnets.

Various methods, such as alloy doping (Li et al., 2022; Chen et al., 2012) and surface modification (Cao et al., 2017; Ouyang et al., 2019); have been employed to improve the corrosion resistance of sintered NdFeB magnets. Alloy doping is a prevalent technique aimed at reducing the potential difference between different phases in the magnet to improve corrosion resistance. However, the addition of alloying elements also brings some drawbacks, including weakened reactivity of the

grain boundary phase, remanence, and magnetic energy product. Surface modification means the application of protective films to isolate the surface of sintered NdFeB from the external environment and corrosive substances, which thereby achieves long-term protection. The electrochemically assisted sol-gel method presents an innovative prospect for fabricating thicker and better anti-corrosive silane films compared to the conventional dipping or spinning techniques. Throughout the electrochemically assisted sol-gel fabrication process, the composition and structure of deposited silane films can be controlled by adjusting electrochemical parameters, such as potential and duration time, enabling customization of the film properties (Collinson, 2007).

Currently, researchers are favoring the sol-gel approach over traditional toxic chromium-based conversion films in the development of the surface protection field owing to its environmentally friendly nature. Some popular employed organic silanes include 1,2-bis(trimethoxysilyl) ethane (BTME) (Rodošek et al., 2024), N-(2-aminoethyl)-3-aminopropyltrimethoxysilane (ATMS) (Vennerberg et al., 2014), tetraethoxysilane (TEOS) (Hamidon and Hussin, 2020), decyltrimethoxysilane (DTMS) (Li et al., 2021); and hexadecyltrimethoxysilane (HDTMS) (Latthe et al.,

* Corresponding author.

E-mail address: jiangli@cjlu.edu.cn (L. Jiang).<https://doi.org/10.1016/j.arabjc.2024.106057>

Received 2 July 2024; Accepted 7 November 2024

Available online 17 November 2024

1878-5352/© 2024 The Authors. Published by Elsevier B.V. on behalf of King Saud University. This is an open access article under the CC BY-NC-ND license (<http://creativecommons.org/licenses/by-nc-nd/4.0/>).

2009); etc. For example, Calabrese et al. (Calabrese et al., 2015) designed a multilayering silanization procedure on NdFeB substrate and demonstrated its excellent corrosion resistance. Based on Chen et al. (Chen et al., 2021) results, superhydrophobic coating could be formed by spraying the mixture of ZnO whisker (T-ZnOw) and polydimethylsiloxane (PDMS) onto the surface of the materials, and the composite coating can significantly improve the anticorrosion capabilities of sintered NdFeB magnets. The main characteristic of silane is the formation of a metal-siloxane bond (Si–O–Me) on the substrate surface, which can effectively anchor the silane layer to the underlying metal and consequently create a protective barrier against corrosive agents. Moreover, previous research (Ramezanzadeh et al., 2015) reported that dual-component silane films exhibited enhanced corrosion resistance and durability compared to their single-component counterparts, which thereby significantly bolstered the stability of the silane solution and offered superior corrosion protection to the metal substrate through their synergistic effect (Metroke et al., 2009; Costenaro et al., 2017). Nevertheless, network structure films composed of silanol groups are inadequate in providing corrosion protection as some micropores and cracks will be produced from water evaporation during the curing process (Santana et al., 2016). To ensure long-term protective performance, it is necessary to incorporate corrosion inhibitors into the electrochemically assisted sol-gel fabricated silane films.

Some previous investigations have demonstrated that the barrier property of the silane film can be enhanced by incorporating nanomaterials, such as graphene oxide (Xue et al., 2017), titania nanoparticles (Purcar et al., 2019), and rare earth salt (Asadi et al., 2014; Motte et al., 2012; Taheri et al., 2017). Incorporating various doping species, such as inhibitors, in small quantities can alter the chemical, morphological, and protective properties of films. For example, rare earth salts are used as corrosion inhibitors due to their ability to precipitate as insoluble hydroxides on cathodic sites, thereby impeding or even completely blocking corrosion activity in damaged areas of hybrid films (Fedel et al., 2017). This phenomenon can significantly extend the service life of the film. Additionally, the rare earth salt-modified silane films exhibited improved barrier properties due to reduced porosity, increased thickness, and decreased conductivity (Wu et al., 2010). Xu et al. (Xu et al., 2023) reported that cerium nitrate and BTESPT silane composite conversion coatings were successfully prepared on the surface of Mg-Li alloy; which effectively prevents corrosive medium from contacting with substrate surface. Based on Adriaens et al. (Zand et al., 2016) results, silane films formed using GPTMS filled with cerium salt activated CeO₂-SiO₂ nanoparticles revealed improved barrier properties compared with the blank steel substrates. Alongside cerium salt, the integration of lanthanum salt as a corrosion inhibitor into the silane film can also enhance the film's stability and corrosion resistance. Meanwhile, it is known that lanthanides exhibit lower toxicity than other rare earth elements and do not pose health risks when used (Toorani et al., 2017). Lanthanum salts also possess excellent oxidation inhibition properties, which are capable of preventing the degradation of silicon films during their usage. Compared with pure GPTMS/TEOS silane film, the lanthanum-doped silane film exhibited a denser structure that was devoid of microcracks and significantly enhanced corrosion resistance (Guin et al., 2014). Furthermore, the primary organic groups in the lanthanum-doped silane film showed no significant divergence from those in the undoped sample (Qiao et al., 2015).

In this study, we present a simple, practicable, and cost-effective technique for fabricating an excellent anti-corrosive lanthanum-silane (DTMS/TEOS) film on sintered NdFeB substrate. The role of incorporated lanthanum salt in tailoring the microstructure and effecting on corrosion and magnetic properties were studied. The lanthanum-silane (DTMS/TEOS) film has outstanding corrosion resistance and superhydrophobicity, and has little influence on the magnetic properties of the substrate. Moreover, the lanthanum-silane (DTMS/TEOS) film forming mechanism and anti-corrosion mechanism on sintered NdFeB were also discussed.

2. Experimental

2.1. Materials

Dodecyltrimethoxysilane (DTMS, AR grade) was procured from Macklin (China). Tetraethoxysilane (TEOS, AR grade) and lanthanum nitrate (La(NO₃)₃, AR grade) were sourced from Kemiou (China). Sintered NdFeB samples with a size of 35.0 mm × 10.0 mm × 2.0 mm were obtained from Hengdian Group DMEGC Magnetics Co., Ltd. The surface of the sintered NdFeB samples was initially treated with a progressive polishing regimen employing 500, 800, 1000, and 1200-grit sandpaper. After that, ethanol decontamination and subsequent nitrogen drying procedures were administered to the samples.

2.2. Electrochemically assisted sol-gel fabrication of lanthanum-silane film on sintered NdFeB surface

The schematic representation of the electrochemically assisted sol-gel fabrication of lanthanum-silane film on the sintered NdFeB substrate is illustrated in Fig. 1. The precursor solution was composed of DTMS, TEOS, 0.2 M NaNO₃ aqueous solution, and anhydrous ethanol with a volume ratio of 1:1:8:32. Before fabrication, the pH of the above mixture was adjusted to approximately 3.5 and then hydrolyzed for 24 h at 35 °C under magnetic stirring. The quantity of added lanthanum nitrate was maintained at 0.15 mol·L⁻¹ based on the concentration of La³⁺ in the solution. The working electrode employed in the electrochemical process was pretreated sintered NdFeB, whereas a platinum sheet with 99.99 % purity and an area of 20.0 mm × 20.0 mm served as the counter electrode. A saturated calomel electrode was utilized as the reference electrode. The deposition was carried out using a CHI660e electrochemical workstation. Unless otherwise stated, the typical deposition potential was -1.4 V and the duration was 300 s. After deposition, the samples were rinsed with absolute ethanol and then dried at 50 °C for 2 h. Pure bis-silane (DTMS/TEOS) films were also prepared using the same method as the lanthanum-silane film, but without the addition of lanthanum nitrate. In order to compare the effect of lanthanum salt on the performance of film, the film samples with the same deposited time and same thickness were all made.

2.3. Characterization

Various analytical techniques were applied to characterize the fabricated pure bis-silane and lanthanum-silane films. Fourier transform infrared spectroscopy (FTIR) was recorded using a Nicolet 470 instrument from Thermo Nicolet, USA, to obtain the types of chemical structures of bis-silane and lanthanum-silane films in the range of 4000–400 cm⁻¹ at room temperature (transmittance mode). X-ray photoelectron spectrometer (XPS) analysis was conducted using a K-Alpha instrument from Thermo Scientific, USA. Secondary ion mass spectrometry (SIMS) investigations were carried out using an IMS-1280HR spectrometer from Cameca, France. The surface microstructures of prepared bis-silane and lanthanum-silane films were examined by scanning electron microscopy (SEM) was performed using a FEI Quanta 650 microscope from FEI, USA. The elemental composition was determined through an energy dispersive spectrometer (EDS) using an Oxford EDS 7426 system from Oxford, UK, was used to study the chemical composition. The surface roughness and profiles of uncoated and coated substrates were measured using a KLA-Tencor stylus P-6 profiler. To assess the surface wettability of the prepared samples, contact angle measurements were conducted using an FCA500B apparatus from Shanghai Power, China.

2.4. Corrosion resistance measurements

The corrosion resistance performance of both the pure bis-silane film and lanthanum-silane film was evaluated using potentiodynamic polarization curves and electrochemical impedance spectroscopy (EIS) in a

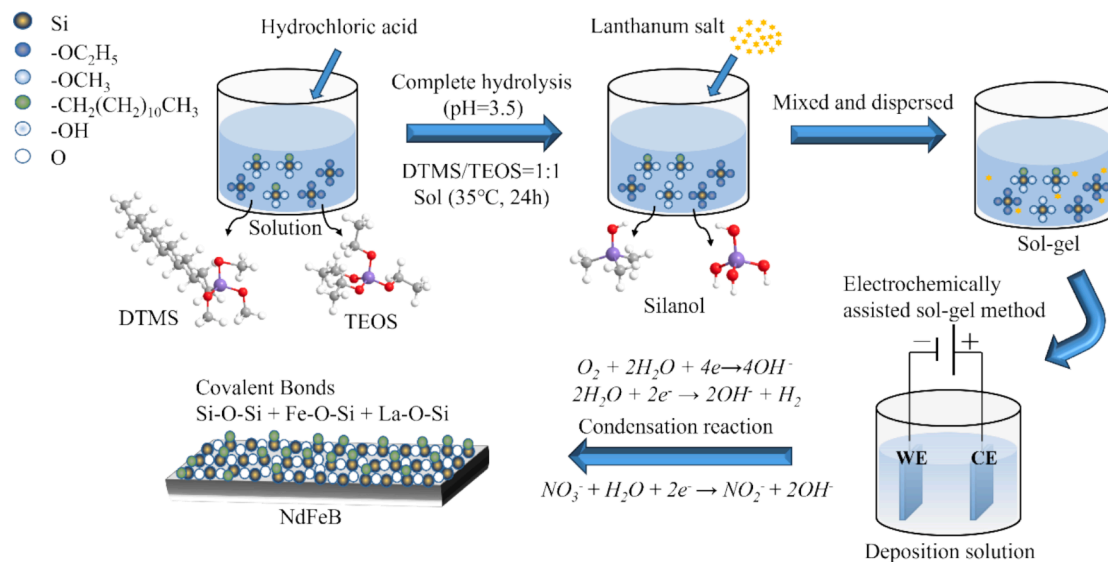


Fig. 1. Schematic diagram of the electrochemically assisted sol-gel fabrication of the lanthanum-silane film onto the sintered NdFeB.

3.5 wt% NaCl solution with a conventional three-electrode cell (as described in Section 2.2). Potentiodynamic polarization curves were obtained by scanning the potential within the range of $E_{ocp} \pm 300$ mV (where E_{ocp} represents the open circuit potential) at a scan rate of $0.1 \text{ mV}\cdot\text{s}^{-1}$. EIS measurements employed a sinusoidal signal with an amplitude of 5 mV in a frequency range from 100 kHz to 10 mHz.

2.5. Magnetic property measurements

The magnetic properties of both the bare sintered NdFeB substrate and the film-coated samples were evaluated utilizing the Physical Properties Measurements System (PPMS-9T, Quantum Design, USA) and Vibrating Sample Magnetometers (LakeShore7404, LakeShore, USA). The effect of the composite film on the magnetic properties of sintered

NdFeB was determined by analyzing the corresponding M-H test curve.

3. Results and discussion

3.1. Characterization of the lanthanum-silane films

FT-IR analyses were conducted to study the chemical structures of the bis-silane and lanthanum-silane films as shown in Fig. 2. The broad peak at approximately 3425 cm^{-1} is attributed to the O-H stretching vibration (Pourhashem et al., 2017). Compared to bis-silane film; the introduction of lanthanum notably diminishes the intensity of the peak. Two prominent peaks at 2930 cm^{-1} and 2841 cm^{-1} correspond to the asymmetric and symmetric stretching of C-H bands in -CH₃ and -CH₂ groups of the alkyl chain in DTMS molecules, respectively (Kirtay, 2014;

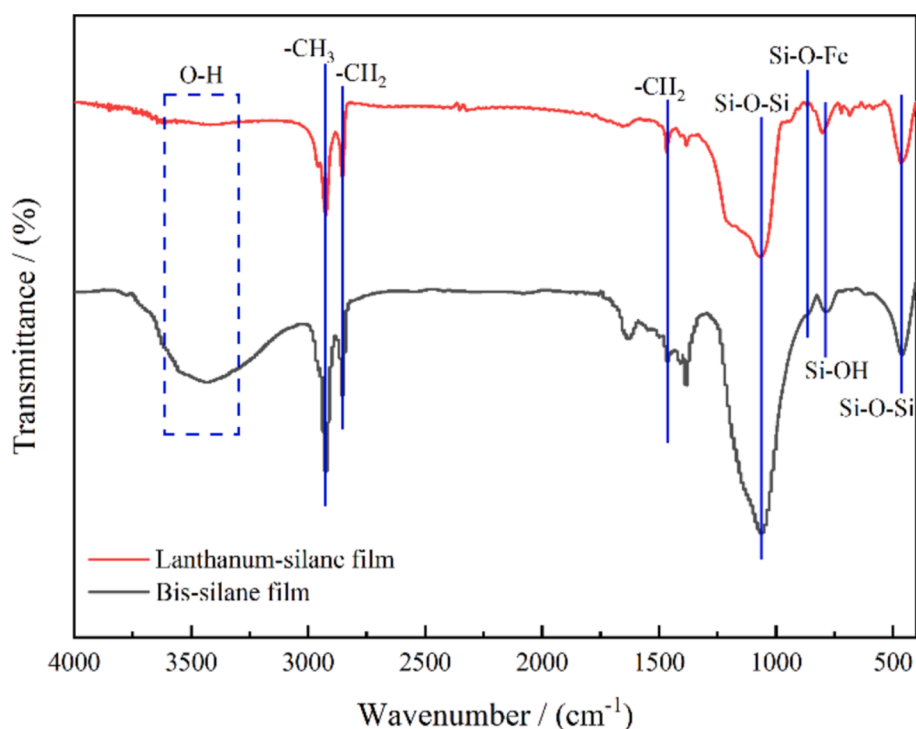


Fig. 2. FT-IR spectra of the fabricated bis-silane and the lanthanum-silane film coated on the sintered NdFeB substrate.

Olivieri et al., 2021). The peak at 1465 cm^{-1} corresponds to $-\text{CH}_2$ of the alkyl chain. The typical intense peak at 1065 cm^{-1} and 467 cm^{-1} represent the Si–O–Si bond formed through the self-condensation reaction of hydrolyzed Si–OH groups. The characteristic peak related to Si–OH stretching can be observed at 789 cm^{-1} ; which results from the incomplete hydrolysis of bis-silane (Fang et al., 2019). Additionally, the weak shoulder peak at 853 cm^{-1} indicates Si–O–Fe vibrations, confirming the successful chemical bonding between the prepared silane film and the sintered NdFeB substrate surface (Hamidon and Hussin, 2020). Therefore, it can be deduced that during the electrochemically assisted sol–gel deposition process, the hydrolyzed Si–OH groups initially form covalent Si–O–Fe bonds at the interface by connecting with Fe–OH groups on the pretreated NdFeB substrate surface, which

remarkably enhances the film adhesion. Then, excess adsorbed Si–OH groups undergo self-condensation, forming a three-dimensional Si–O–Si network on the surface. This network structure subsequently serves as a scaffold for the deposition of lanthanum compounds, which facilitates orderly particle deposition and improves the density and uniformity of the fabricated lanthanum-silane composite film.

SEM graphs were acquired to assess the surface morphology and cross-section morphology of the bis-silane film and the lanthanum-silane film. Fig. 3a shows the surface morphology of the fabricated bis-silane film at various magnifications. It is characterized hierarchical structure. The rough and undulating surface was beneficial to super-hydrophobicity. In comparison, a relatively uniformly distributed and more compact surface without obvious cracks or cavity defects can be

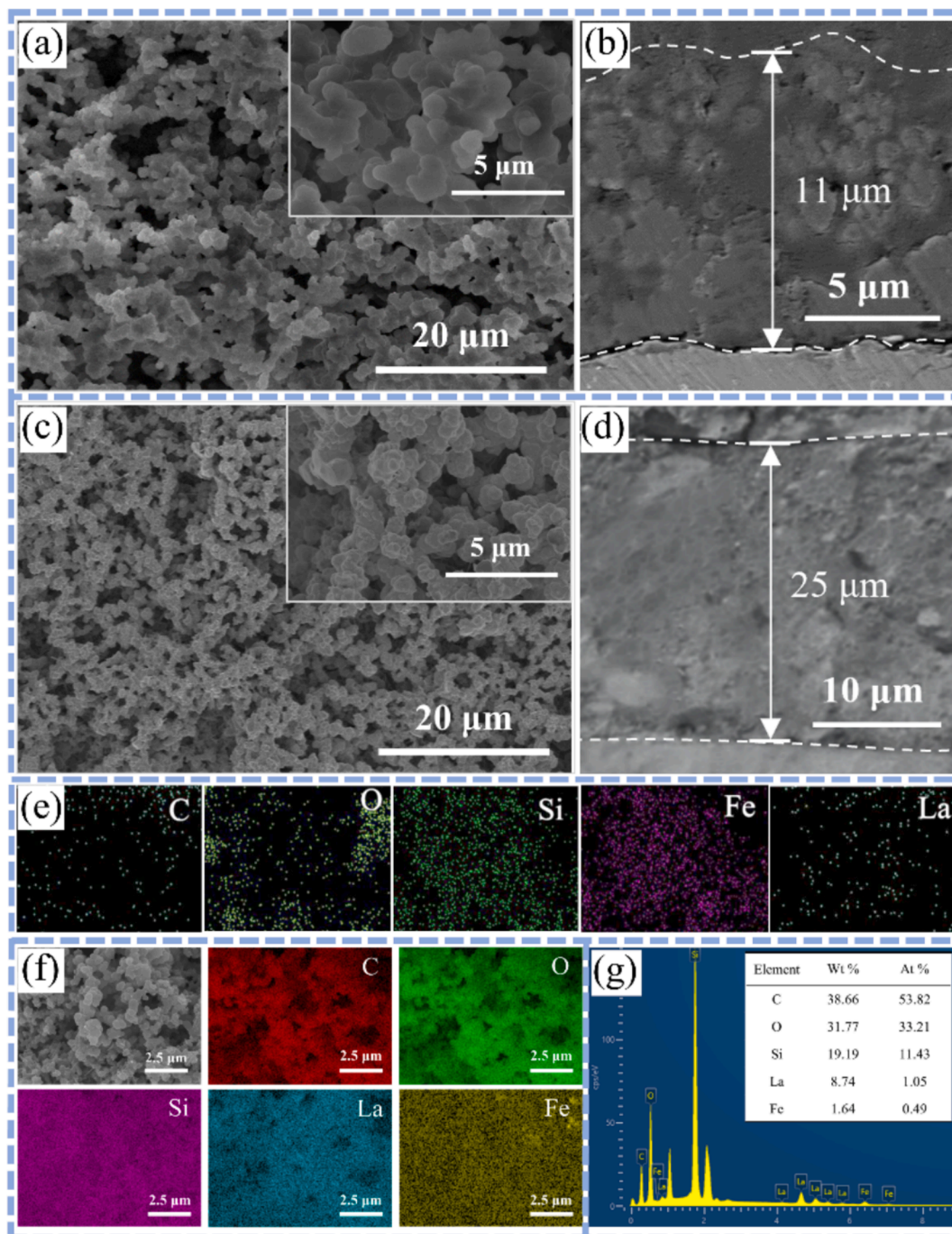


Fig. 3. SEM graphs of the surface and cross-section of the bis-silane film (a, b) and the lanthanum-silane film (c, d); the corresponding element distribution analysis (e) of the lanthanum-silane film's cross-section; the element mappings (f) and EDS (g) results corresponding to the lanthanum-silane film surface.

observed for the prepared lanthanum-silane film (Fig. 3c). Microscopically, the lanthanum-silane film exhibited a tightly bonded structure, featuring a well-defined distribution of interconnected colloidal particles and micelles. In addition, as shown in Fig. 3d, the thickness of the fabricated lanthanum-silane film was approximately 25 μm , which value was much larger than that of the prepared pure silane film (11 μm , in Fig. 3b). This denser and thicker lanthanum-silane film may be ascribed to the positive catalysis effect of added lanthanum on the self-condensation reaction of silanol groups, which was also proved by the above FTIR measurement.

Fig. 3e presents the element distribution analysis of the lanthanum-silane film cross-section, while Fig. 3f and g display the element mapping and EDS results of the film's surface. The results indicate the presence of C, O, Si, Fe, and lanthanum (La) elements in the fabricated lanthanum-silane film. The film primarily consists of C, O and Si elements, with the inclusion of abundant C element that is attributed to the long-chain alkyl groups in the DTMS molecules (Gu et al., 2009; Parhizkar et al., 2017). The existence of La element suggests the successful modification of silane film with lanthanum additive. The diagram illustrates a relatively uniform distribution of C, O, Si, and La elements throughout the composite film. Notably, the distribution of O elements in the lanthanum-silane film adjacent to the sintered NdFeB substrate surface appears much denser than the other areas, implying a higher degree of connectivity at the film/substrate interface.

To characterize the chemical state and constituent elements, XPS result of the lanthanum-silane film are presented in Fig. 4. The full spectrum reveals signals corresponding to C 1s, O 1s, Si 2p, and La 3d, indicating the presence of both deposited silane film and added lanthanum, which agrees well with the element distribution analysis (shown in Fig. 3). As shown in Fig. 4b, the C 1s spectrum is resolved into two peaks associated with C-C and C-Si bonding, centered at 284.5 eV and 285.2 eV, respectively. The high-resolution O 1s spectrum displayed in Fig. 4c exhibits three distinct chemical states, with typical peaks at 530.2 eV, 532.4 eV, and 532.8 eV representing Si-O-Fe, Si-O-Si and SiO₂ bonding, respectively. The characteristic Si-O-Si and Si-O-Fe bonds observed in Fig. 4c further confirm the chemical bonding of deposited siloxane on the sintered NdFeB surface. The presence of SiO₂ bonds suggests the existence of unhydrolyzed silanol or silane, while the Si 2P spectrum in Fig. 4d contains four characteristic peaks at around 99.6 eV, 101.4 eV, 102.6 eV, and 103.6 eV, correlating to Si-O-Fe, Si-C,

Si-O-Si, and SiO₂, respectively (Yang et al., 2012; Zhang et al., 2022). The La 3d spectrum, as shown in Fig. 4e, is composed of six peaks which are assigned to La₂O₃ and La(OH)₃. It is generally accepted that rare earth salts can effectively inhibit the cathode reaction during the metal corrosion process by depositing a partially insoluble oxide or hydroxide film that covers the active corrosion sites, leading to good anti-corrosion performance (Lakshmi and Aruna, 2017). Fig. 4f presents the elemental composition derived from the XPS full spectrum. C element constitutes the majority of the lanthanum-silane film at 52.5 at%, followed by O element (26.3 at%). The elemental content of lanthanum (La) is 1.3 at%, which corresponds closely to that of the EDS results. In the present study, lanthanum oxide and hydroxide fill the voids and crevice defects in the deposited silane film, which efficiently prevents the corrosive electrolytes from diffusion and penetration onto the substrate surface. The above analysis demonstrates that a dense lanthanum-silane composite film was firmly attached to the sintered NdFeB substrate surface by the electrochemically assisted sol-gel method.

As a powerful surface analytical technique, Secondary Ion Mass Spectrometry (SIMS) is capable of supplying precise acquisition of concentration profiles for elements (Anischik et al., 2005). In Fig. 5, the SIMS chemical maps of the lanthanum-silane film reveal an even distribution of CH⁺, Si⁺, SiO⁺, and SiHO⁺ bonds from the silicon-oxygen network on the matrix surface, which suggests the absence of noticeable defects in the prepared film. Additionally, a uniform distribution of FeO⁺ bonds is observed, indicating the formation of metal-siloxane bond (Si-O-Fe), which is in good accordance with the above FTIR and XPS result. This covalent bond anchors the silane layer effectively to the underlying metal, thereby enhancing the adhesion of the coating, which is a significantly important factor that affects long-term corrosion protection performance. The distribution of LaO⁺ exhibits a slightly regional aggregation pattern. Comparative analysis reveals that lanthanum compounds are predominantly interleaved with silicon-oxygen networks, which demonstrates that the deposited lanthanum compounds fill some defects in the bis-silane film, thereby forming a denser structure and enhancing the physical barrier properties of the composite film.

3.2. Surface wettability measurements

To investigate the influence of incorporated lanthanum salt on the

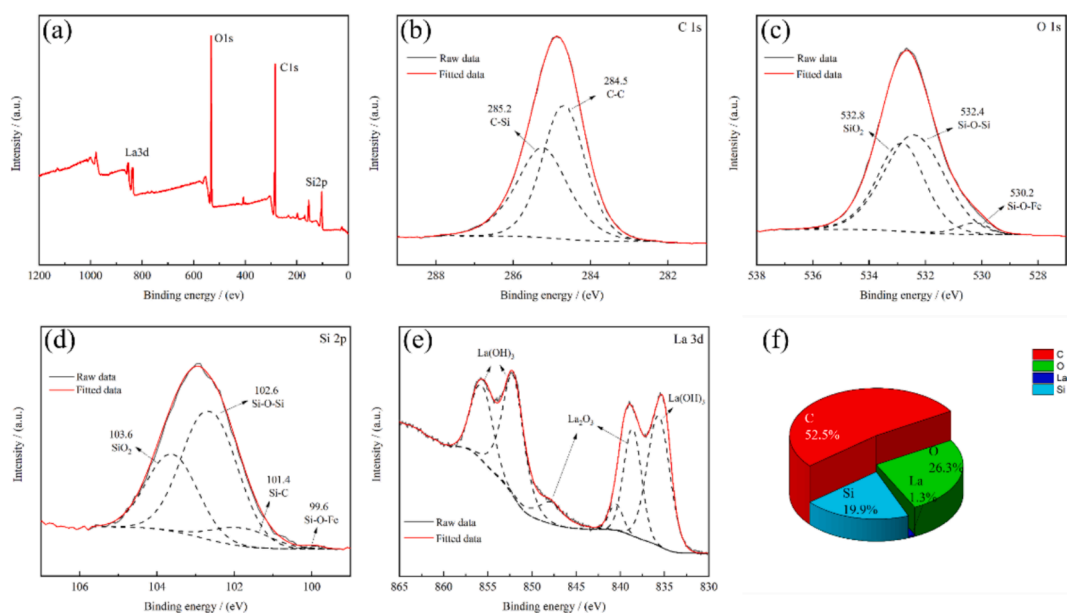


Fig. 4. XPS result of the lanthanum-silane film, full spectrum (a) and high-resolution spectra for individual elemental regions: C 1s (b), O 1s (c), Si 2p (d), and La 3d (e), and the percentage of elements corresponding to full spectrum (f).

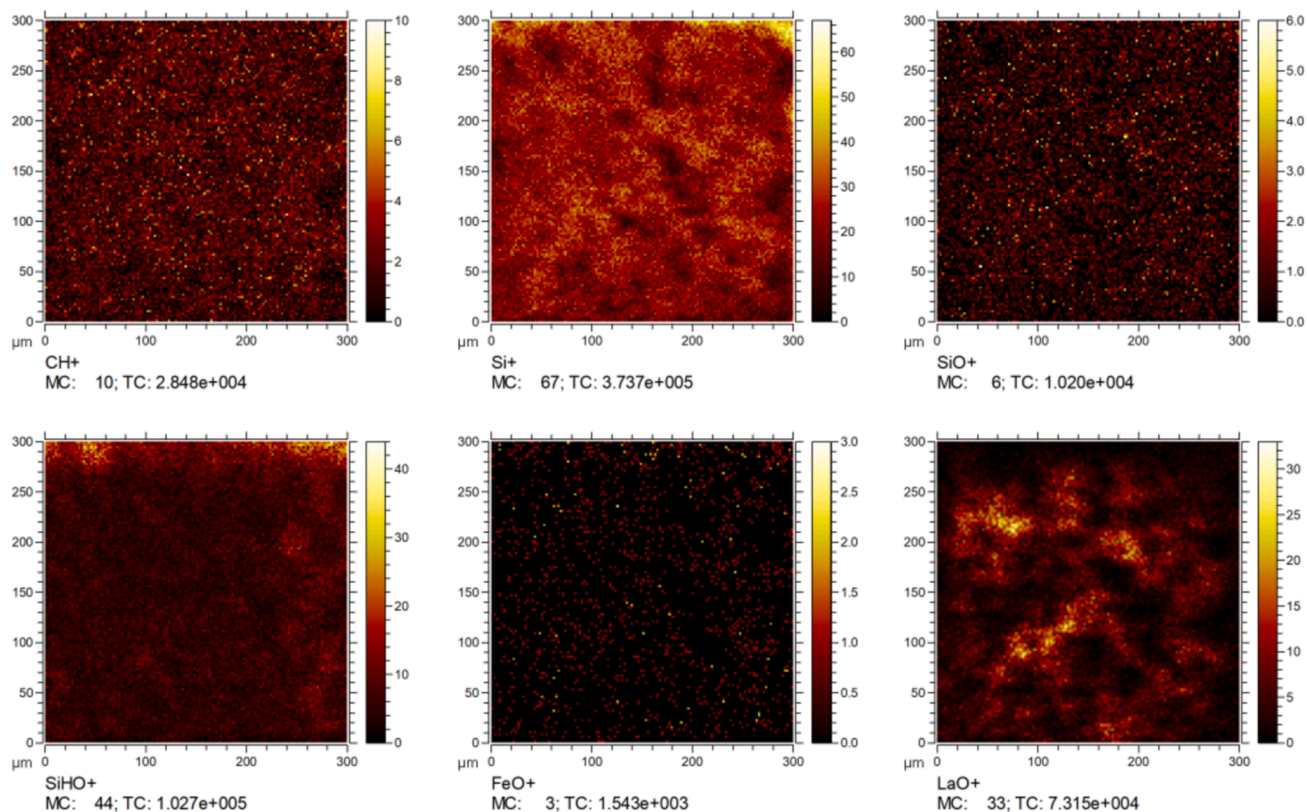


Fig. 5. Chemical maps obtained via SIMS for the surface of the lanthanum-silane film.

hydrophobicity of silane film, the contact angles of the sintered NdFeB, the bis-silane film, and the lanthanum-silane film were measured, as shown in Fig. 6. The results revealed that the contact angles for the bis-silane and the lanthanum-silane film were 153° and 151° , respectively. The exceptional superhydrophobicity of the bis-silane film stems from a synergistic interplay between surface roughness and low surface energy. This is primarily induced by the long non-hydrolytic alkyl chains that are presented in DTMS molecules. Furthermore, the formation of silica

particles from TEOS monomers further enhances surface roughness, thereby reinforcing its hydrophobic properties (Beirami et al., 2020). The smaller contact angle of the lanthanum-silane film may be related to its smoother and more compact surface (Nakajima, 2011). The addition of lanthanum salt to the composite film led to the distribution of lanthanum ions within the silane network. This resulted in the filling up of the space between the silica particles to some extent (Telmenbayar et al., 2022). Fig. 6b–d show the profiles of three materials: sintered

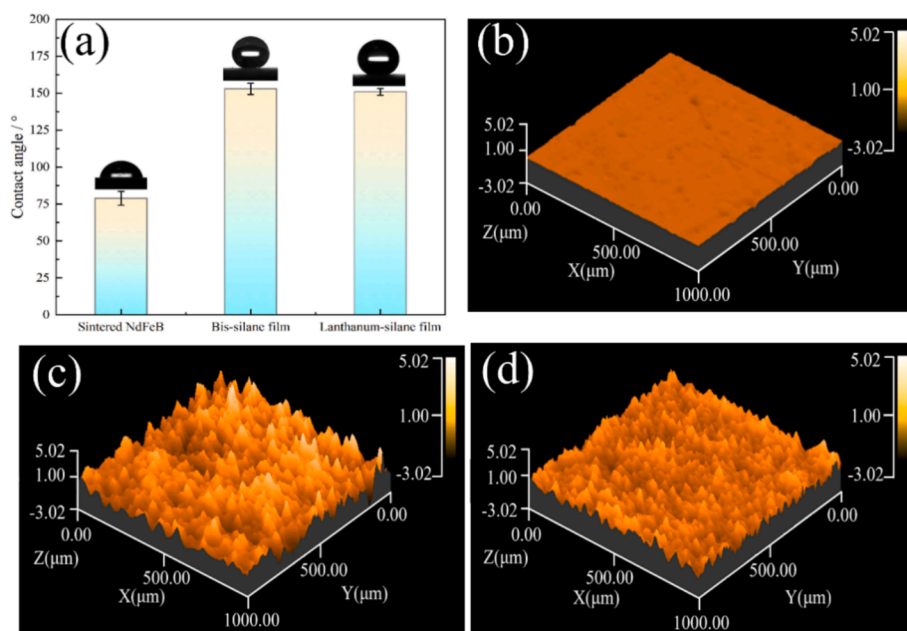


Fig. 6. Contact angle measurements for the samples (a); the profiles of sintered NdFeB (b), bis-silane film (c), and lanthanum-silane film (d).

NdFeB, bis-silane film, and lanthanum-silane film. The lanthanum-silane film had a lower Ra value of surface roughness (0.48 μm) as compared to the bis-silane film (0.59 μm). The remarkable superhydrophobic properties of the lanthanum-silane film stem from its capacity to trap significant volumes of air on the surface. This results in exceptional water repellence and reduces the likelihood of corrosive media infiltration (Zhang et al., 2015; Buijnsters et al., 2013).

3.3. Corrosion resistance measurements

To compare the corrosion resistance of film-coated and uncoated samples, we prepared a bis-silane film with a thickness comparable to that of the la-silane film. The thickness of the silane film was increased to

23 μm by adjusting deposition parameters (deposition time), and the thickness of lanthanum-silane film was about 25 μm . The corrosion resistance of the specimens was investigated through electrochemical techniques. The potentiodynamic polarization plots and EIS results for the samples immersed in a 3.5 wt% NaCl solution are presented in Fig. 7. Some informative Tafel parameters, including corrosion potential (E_{corr}), corrosion current density (I_{corr}), anodic slope (β_a), and cathodic slope (β_c), were deduced from the potentiodynamic polarization curve using the extrapolation method. The obtained values are summarized in Table 1. The corrosion protection efficiency (η) was determined by utilizing the following equation (Liu et al., 2016), and the calculated results were also listed in Table 1.

$$\eta = (I_{corr}^0 - I_{corr}^1) / I_{corr}^0 \times 100\% \quad (1)$$

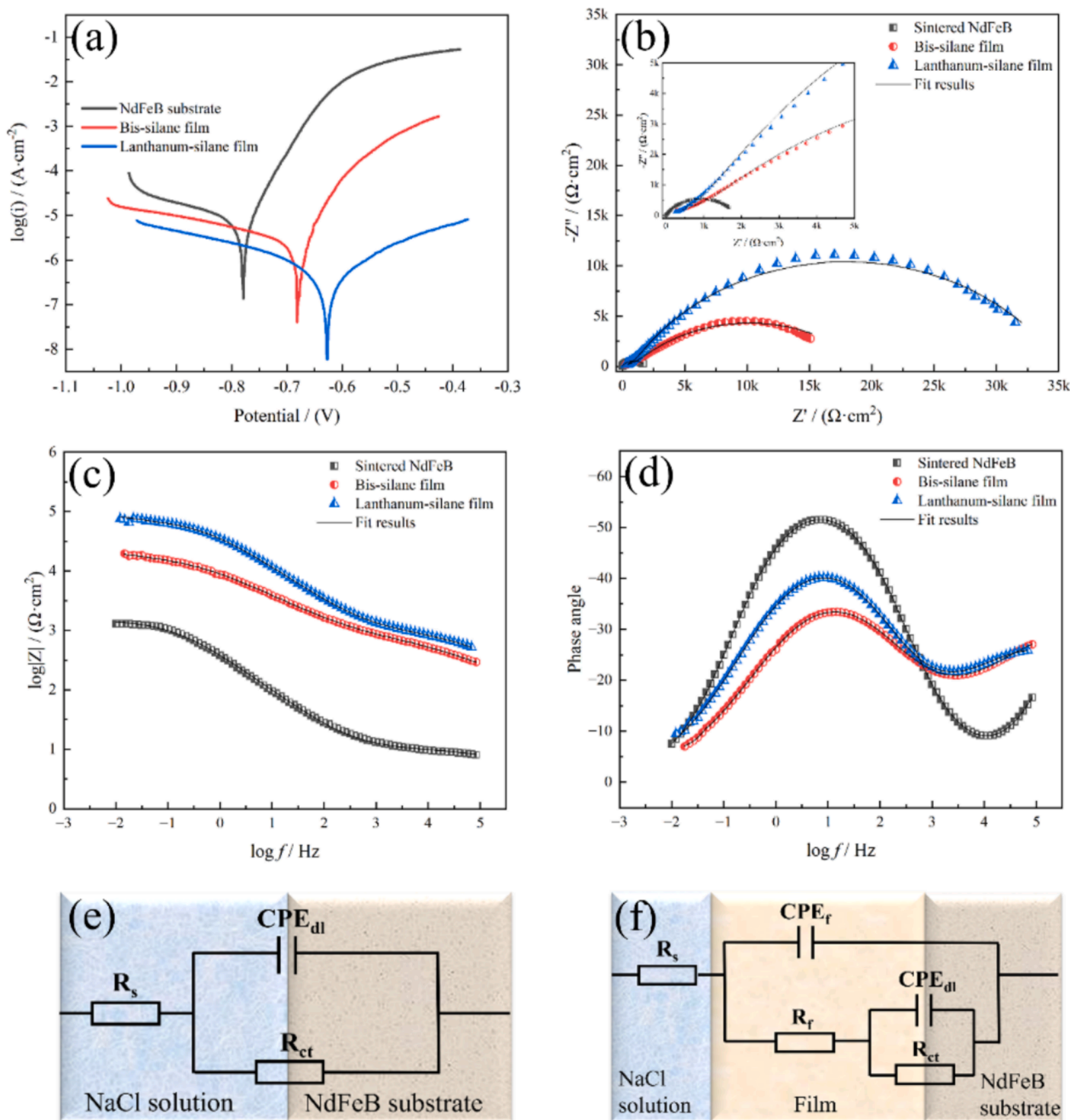


Fig. 7. The potentiodynamic polarization plots (a), Nyquist plots (b), Bode plots(c), and phase angle plots (d) for the sintered NdFeB, the bis-silane film-coated sample, and the lanthanum-silane film-coated sample immersed in 3.5 wt% NaCl solution; Corresponding equivalent electric circuits for the sintered NdFeB (e) and film-coated samples (f).

Table 1

The electrochemical parameters of polarization curves for the sintered NdFeB, the bis-silane film-coated sample, and the lanthanum-silane film-coated sample in a 3.5 wt% NaCl solution.

Sample	E_{corr} (V)	I_{corr} (A·cm ⁻²)	$-\beta_c$ (mV·dec ⁻¹)	β_a (mV·dec ⁻¹)	$\eta\%$
Sintered NdFeB	-0.779	7.09×10^{-6}	296	51.2	/
Bis-silane film-coated sample	-0.682	2.02×10^{-6}	311	57.8	71.5 %
Lanthanum-silane film-coated sample	-0.627	5.26×10^{-7}	196	166	92.5 %

where, I_{corr}^1 and I_{corr}^0 correspond to the corrosion current densities of sintered NdFeB with and without films, respectively. The E_{corr} values of the sintered NdFeB, the bis-silane film-coated sample, and the lanthanum-silane film-coated sample were -0.779, -0.682, and -0.627 V, respectively. Notably, the corrosion potential of the electrochemically assisted sol-gel films exhibited a positive shift, indicating increased stability with a thermodynamically slower corrosion rate for both the bis-silane film-coated sample and the lanthanum-silane film-coated sample. Meanwhile, the current densities of both the anodic and cathodic branches decrease, suggesting that the fabricated films effectively suppressed both the anodic Fe dissolution reaction and the cathodic oxygen reduction rate. Compared to the corrosion current density of the sintered NdFeB (7.09×10^{-6} A cm⁻²), the corrosion current density of the bis-silane film-coated sample is 2.02×10^{-6} A cm⁻² and the lanthanum-silane film coated sample is 5.26×10^{-7} A cm⁻². Consequently, the η values of the bis-silane film and lanthanum-silane film-coated samples were calculated to be 71.5 % and 92.5 %, respectively. This outcome highlights that the lanthanum-doped bis-silane film significantly enhances the corrosion resistance of the sintered NdFeB substrate in NaCl electrolyte (Duan et al., 2023).

EIS is a non-destructive and convenient technique and was used for evaluating the corrosion behaviors of metals. The measured EIS data were fitted using Z-view software, and the analyzed data were presented in Table 2. In the proposed equivalent electrical circuit, R_s represents solution resistance, R_{ct} signifies charge transfer resistance, R_f corresponds to film resistance, CPE_f , and CPE_{dl} are related to film capacitance and double-layer capacitance, respectively. Constant Phase Element (CPE) was employed instead of the ideal capacitor (C) to account for surface heterogeneity and roughness. The impedance of the CPE element (Z_{CPE}) can be modeled by the following equation:

$$Z_{CPE} = 1/Q(j\omega)^n \quad (2)$$

where, the parameters Q , n , and ω represent the CPE constant, CPE exponent, and angular frequency, respectively. The total resistance (R_t) comprises R_f and R_{ct} as follows,

$$R_t = R_f + R_{ct} \quad (3)$$

The Nyquist plot of the lanthanum-silane film-coated sample exhibits a larger capacitive arc radius, indicating that the incorporation of lanthanum salt enhances corrosion resistance (inset in Fig. 7b) (Zhong et al., 2019). As depicted in Fig. 7c, the sintered NdFeB exhibits the lowest impedance value in the low-frequency region, which is indicative

Table 2

The electrochemical parameters of EIS plots for the sintered NdFeB, the bis-silane film-coated sample, and the lanthanum-silane film-coated sample in a 3.5 wt% NaCl solution.

Sample	R_s (Ω ·cm ²)	CPE_{dl} (Ω^{-1} S ⁿ ·cm ⁻²)	n_1	R_{ct} (k Ω ·cm ²)	CPE_f (Ω^{-1} S ⁿ ·cm ⁻²)	n_2	R_f (k Ω ·cm ²)	R_t (k Ω ·cm ²)
Sintered NdFeB	5.1	1.39×10^{-5}	0.70	1.87	/	/	/	1.87
Bis-silane film-coated sample	4.4	8.37×10^{-6}	0.71	2.02	6.28×10^{-6}	0.56	17.79	19.81
Lanthanum-silane film-coated sample	8.3	2.32×10^{-7}	0.66	5.92	1.15×10^{-6}	0.63	38.65	44.57

of its susceptibility to corrosion in a 3.5 wt% NaCl solution. In contrast, the lanthanum-silane film-coated sample presents the highest impedance value in the low-frequency region, revealing its excellent efficacy as a high-impedance barrier layer on the sintered NdFeB. Fig. 7d suggests that the lanthanum-silane film-coated sample possesses an extended line with the phase angle across a broad spectrum of frequencies. This observation underscores the outstanding capacity of the silane matrix and filled lanthanum nanoparticles in the silane network to counteract aggressive ions and corrosive media during the corrosion process (J. TANG, Y. YAO, M. GUO, J. JIANG, H. CONG, Y. CHEN, Y. SUN, Y. KONG, S. HAN, ANTICORROSION AND REPAIR BEHAVIOR OF REC-SiO₂ SILANE FILM ON CARBON STEEL, 28, 2021). Furthermore, the values of R_{ct} (5.92 k Ω cm²) and R_f (38.65 k Ω cm²) of the lanthanum-silane film-coated sample are significantly larger than those for the sintered NdFeB and the bis-silane film-coated sample. And the R_t values for the bis-silane film and the lanthanum-silane film-coated samples are approximately 19.81 k Ω cm² and 44.57 k Ω cm², respectively. This phenomenon demonstrates not only the excellent physical barrier performance of the lanthanum-silane film but also its good inhibitive effect on corrosion reactions (Dias et al., 2014). Simultaneously, both the film capacitance (CPE_f) and electrical double layer capacitance (CPE_{dl}) for the lanthanum-silane film are lower than those for the bis-silane film, indicating that the prepared lanthanum-silane film possesses superior water barrier properties and a minimal contact area with the corrosive electrolyte at the interface (Yang et al., 2021). This observation indicates that the lanthanum-silane film offers superior corrosion protection for the sintered NdFeB substrate.

SEM images of the bis-silane film and lanthanum-silane film before the immersion in a 3.5 wt% NaCl solution, demonstrate that the surfaces of both films retain their integrity, with no visible corrosion (as shown in Fig. 8a, b). Additionally, the corrosion resistance R_f value (refer to Table 3) for the lanthanum-silane film-coated sample (38.65 k Ω cm²) is higher than that of the bis-silane film-coated sample (16.48 k Ω cm²). After 48 h of immersion, the SEM image of the bis-silane film reveals numerous corrosion pits, some of which contain cracks and areas where the surface has deteriorated (shown in Fig. 8b). In contrast, the surface of the lanthanum-silane film remains smooth and intact after 48 h of immersion (shown in Fig. 8d). Additionally, the diameter of the capacitive arc decreased for the film-coated samples compared to the 0 h immersion time, indicating a moderate reduction in protective behavior after prolonged exposure (Zhang et al., 2024). Notably, the R_t values decreased by 31.9 % and 15.1 % for the bis-silane film and lanthanum-silane film, respectively, as the exposure time was extended from 0 h to 48 h. Comparing of the SEM images and EIS results indicates that the lanthanum-silane film significantly improves the corrosion resistance of the sintered NdFeB substrate.

Fig. 9 schematically illustrates the forming mechanism and anti-corrosion mechanism of the lanthanum-silane film on sintered NdFeB. Following adequate hydrolysis, the majority of silane molecules in the electrolyte are hydrolyzed into silanol monomers. The silanol monomer undergoes a condensation reaction, connecting to create a closely-knit three-dimensional network structure, wherein the silicon-oxygen bridge serves as the linkage (Foroozan and Naderi, 2015). During the electrochemically assisted sol-gel process, localized alkali catalysis induces metal hydroxylation (MeOH) on the cathodic surface, which facilitates the spontaneous adsorption of silanol molecules on the NdFeB

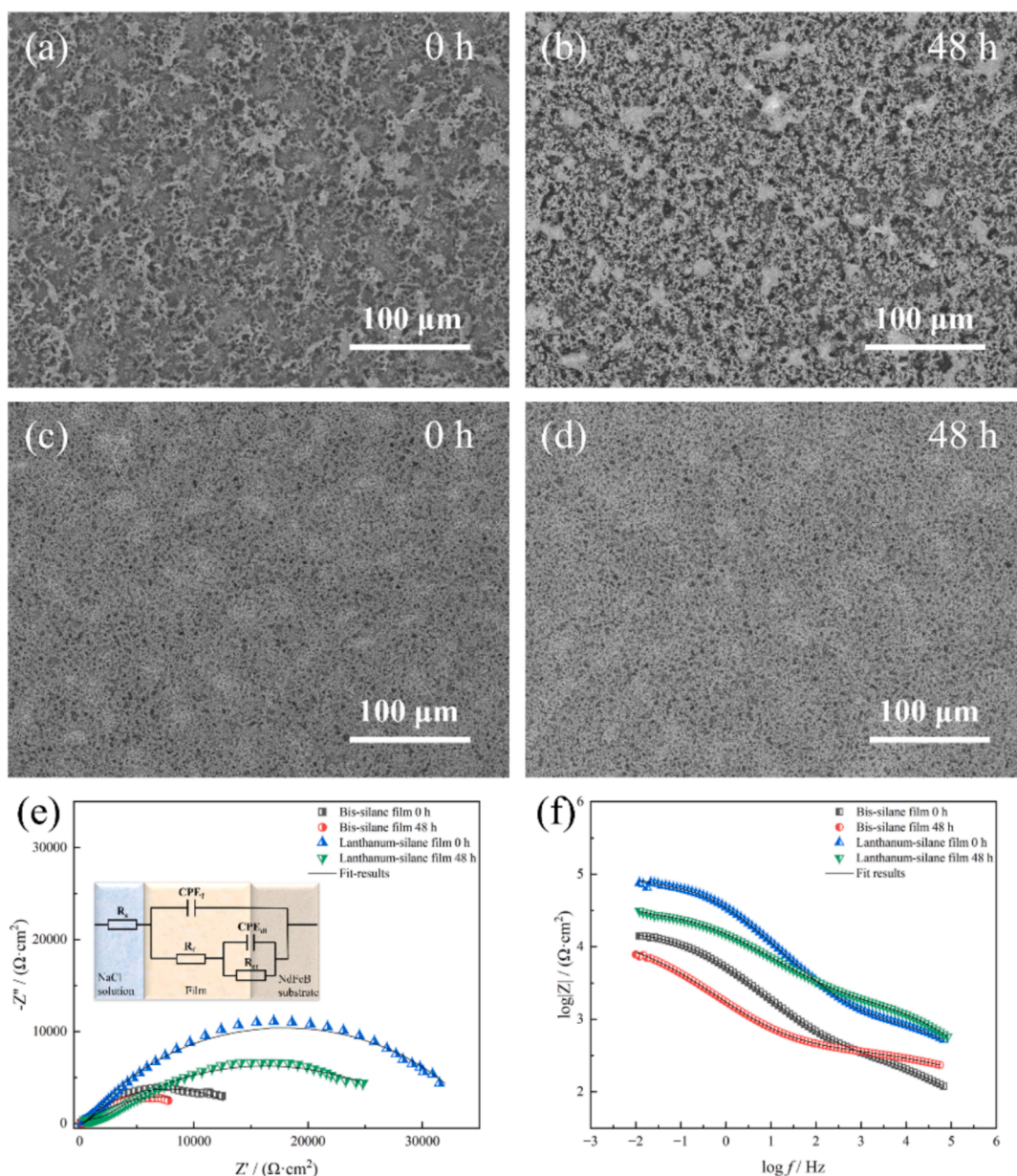


Fig. 8. Surface morphology evolution of the sintered NdFeB coated with bis-silane film (a, b) and lanthanum-silane film (c, d) in 3.5 wt% NaCl solution during different immersion times; The corresponding EIS curves and corresponding equivalent electric circuit (e, f) of the film-coated samples.

Table 3

Results of the EIS fitting for the sintered NdFeB coated with the bis-silane film and lanthanum-silane film during different immersion time.

Sample	R_s ($\Omega\text{-cm}^2$)	CPE_{dl} ($\Omega^{-1}\text{S}^n\text{-cm}^{-2}$)	n_1	R_{ct} ($\text{k}\Omega\text{-cm}^2$)	CPE_f ($\Omega^{-1}\text{S}^n\text{-cm}^{-2}$)	n_2	R_f ($\text{k}\Omega\text{-cm}^2$)	R_t ($\text{k}\Omega\text{-cm}^2$)
Bis-silane film-coated sample-0 h	5.5	2.23×10^{-5}	0.65	1.91	3.52×10^{-5}	0.60	16.48	18.39
Bis-silane film-coated sample-48 h	4.6	4.21×10^{-5}	0.71	0.89	8.37×10^{-5}	0.56	11.63	12.52
Lanthanum-silane film-coated sample-0 h	8.3	2.32×10^{-7}	0.66	5.92	1.15×10^{-6}	0.63	38.65	44.57
Lanthanum-silane film-coated sample-48 h	5.6	8.03×10^{-6}	0.68	4.69	4.87×10^{-6}	0.65	33.16	37.85

surface and the formation of metal-siloxane covalent bonds (Si–O–Fe) (Wu et al., 2013). Concurrently, La^{3+} ions in the solution will be converted to $\text{La}(\text{OH})_3$ precipitates in alkaline conditions in the silane film. Throughout the curing progress, a portion of $\text{La}(\text{OH})_3$ dehydrates, leading to the formation of La_2O_3 . The presence of lanthanum oxide and hydroxide can inhibit the cathodic reaction and consequently impede the corrosion rate. Additionally, $\text{La}(\text{OH})_3$ and La_2O_3 are impermeable, which hinders the penetration of the corrosive medium and leads to the

barrier effect. Furthermore, silanol molecules in the solution react with $\text{La}(\text{OH})_3$ to establish a metal-siloxane covalent bond (Si–O–La), resulting in a more compact composite film (Fan et al., 2017; Saji, 2019). The synergistic effect of the superhydrophobic surface and the physical barrier provided by the dense composite film against corrosive agents significantly enhances the corrosion resistance of the sintered NdFeB substrate, making it suitable for potential applications in challenging environments.

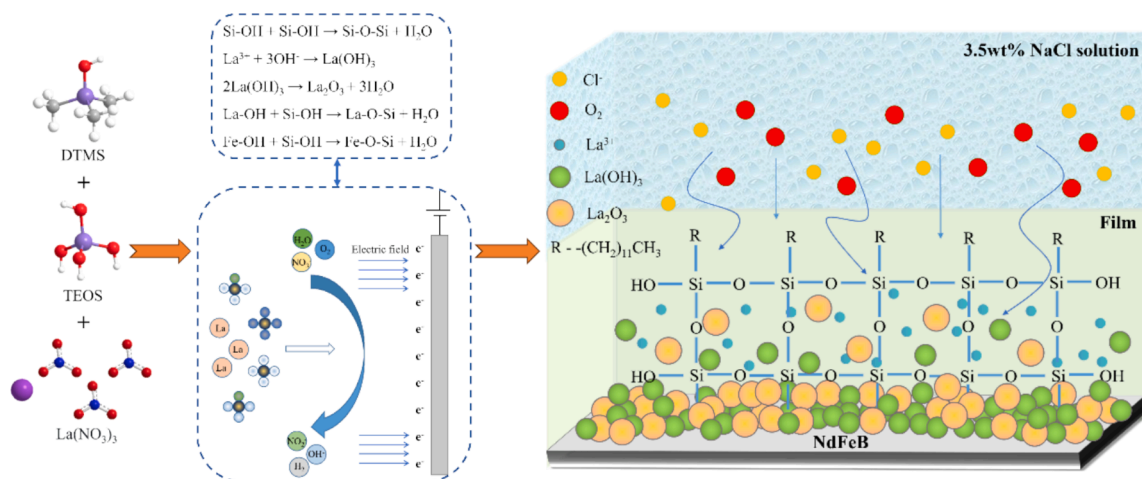


Fig. 9. The schematic diagram for the forming mechanism and anti-corrosion mechanism of the lanthanum-silane film on sintered NdFeB.

3.4. Magnetic properties measurements

Considering that sintered NdFeB magnets are inherently permanent materials in practical applications, it becomes crucial to evaluate the influence of deposited lanthanum-silane film on their magnetic properties. Fig. 10 presents the hysteresis loops of both the lanthanum-silane film-coated and uncoated sintered NdFeB samples, and the corresponding magnetic properties are summarized in Table 4. It is noticeable that the hysteresis loops for both the bare sintered NdFeB substrate and the film-coated samples almost overlap with each other, indicating a negligible influence of the protective film on the intrinsic magnetic properties of the NdFeB magnet. In contrast to the sintered NdFeB, the samples coated with bis-silane and lanthanum-silane films exhibit slight reductions in coercivity (H_{cj}) of approximately 1.57 % and 0.29 %, respectively. The remanent magnetism (B_r) and the maximum magnetic energy product ($(BH)_{max}$) of the bis-silane film-coated sample decrease

Table 4

Magnetic properties of the bare sintered NdFeB and the film-coated samples.

Sample	$B_r(T)$	$(BH)_{max}$ ($\text{kJ}\cdot\text{m}^{-3}$)	H_{cj} ($\text{kA}\cdot\text{m}^{-1}$)
Sintered NdFeB	1.282	329	1016
Bis-silane film-coated sample (Reduction rate, %)	1.267 (-1.17 %)	324 (-1.52 %)	1000 (-1.57 %)
Lanthanum-silane film-coated sample (Reduction rate, %)	1.279 (-0.23 %)	326 (-0.91 %)	1013 (-0.29 %)

slightly, whereas the lanthanum-silane film-coated sample maintains values nearly identical to those of the sintered NdFeB. The results of the literature research on various protective films on the NdFeB substrate are presented in Table 5. The lanthanum-silane film applied to sintered

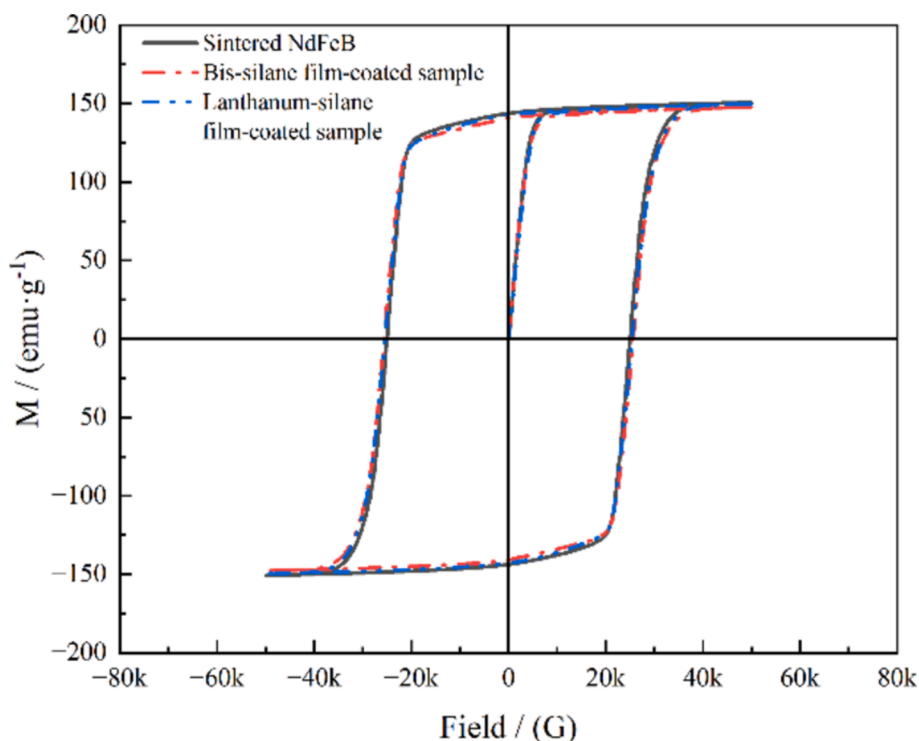


Fig. 10. Hysteresis loops of the bare sintered NdFeB and the film-coated samples.

Table 5
Comparison of various protective films on the NdFeB substrate from literature.

Coating methods	Coating materials	Corrosion current density ($A \cdot cm^{-2}$)	Coercivity variation ($kA \cdot m^{-1}$)	Hydrophobicity	References
Spraying	T-ZnOw/PDMS coating	2.797×10^{-6}	-2.1 %	Superhydrophobic	(Chen et al., 2021)
DC magnetron sputtering	AlN/Al dual coating	1.903×10^{-5}	+0.6 %	/	(Li et al., 2009)
Dipping	Al-Cr coating	/	+0.8 %	/	(Zheng et al., 2012)
Jet electrodeposition	Nickel coating	3.58×10^{-6}	/	/	(Shen et al., 2017)
Ion-beam-assisted-deposition	Cr ₂ O ₃ coating	8.17×10^{-7}	/	/	(Ding et al., 2016)
Electrodeposition	Zinc coatings	7.9×10^{-7}	/	/	(Cao et al., 2015)
Vapor-phase deposition	Phosphate conversion coating	8.26×10^{-7}	/	/	(Zhang et al., 2022)
Cathodic electrophoretic deposition	TCNTs/epoxy coating	5.281×10^{-11}	/	/	(Yang et al., 2022)
Cathode electrophoresis	CeO ₂ /epoxy resin coating	6.479×10^{-8}	+0.28 %	/	(Zhang et al., 2018)
Electrochemically assisted sol-gel	Lanthanum-silane film	5.26×10^{-7}	-0.29 %	Superhydrophobic	This study

NdFeB has demonstrated remarkable properties. It exhibits a lower corrosion current, is superhydrophobic, and does not significantly affect the magnetic properties. These desirable characteristics make it a highly promising option for practical applications involving sintered NdFeB.

4. Conclusion

Bis-silane films doped with lanthanum salt were successfully fabricated onto sintered NdFeB using the electrochemically assisted sol-gel method. Characterization results indicated the successful co-deposition of silane film and La oxide/hydroxide on sintered NdFeB substrate. The silane film chemically bonded with the NdFeB surface through Si-O-Fe bonds. The thickness of lanthanum-silane film was approximately 25 μm , and the contact angle reached 151°, suggesting an excellent super-hydrophobicity. The corrosion potential of the electrochemically assisted sol-gel fabricated films notably shifted in a positive direction. In comparison with the sintered NdFeB, the I_{corr} of the lanthanum-silane film-coated sample decreased significantly from $7.09 \times 10^{-6} A \cdot cm^{-2}$ to $5.26 \times 10^{-7} A \cdot cm^{-2}$ and the protection efficiency reached 92.5 %, which was attributed to the synergistic effect of the super-hydrophobicity coupled with the sealing function of the incorporated lanthanum salt. Importantly, the lanthanum-silane film exhibited no discernible impact on the magnetic properties of the sintered NdFeB substrate.

CRedit authorship contribution statement

Zhu Tao: Writing – original draft, Visualization, Validation, Investigation, Formal analysis. **Li Jiang:** Writing – review & editing, Supervision, Resources, Project administration, Methodology, Funding acquisition, Conceptualization. **Wentao Ju:** Investigation, Formal analysis. **Yanxia Liang:** Validation. **Yumeng Yang:** Funding acquisition. **Guoyang Wei:** Funding acquisition. **Yu Chen:** Funding acquisition, Data curation. **Zhao Zhang:** Resources, Methodology.

Declaration of competing interest

The authors declare that they have no known competing financial interests or personal relationships that could have appeared to influence the work reported in this paper.

Acknowledgments

The authors gratefully acknowledge the financial support from the Public Welfare Projects of Zhejiang Province (Grant No. LGG22E010002), the Innovation Team Project for Colleges and Universities of Guangdong Province (2023KCXTD030), and the National Natural Science Foundation of China (Grants No. 52001300 and 52171083).

References

- Anischik, V.M., Uglov, V.V., Zlotski, S.V., Konarski, P., Cwil, M., Ukhov, V.A., 2005. SIMS investigation of nitride coatings. *Vacuum* 78, 545–550.
- Asadi, N., Naderi, R., Saremi, M., 2014. Effect of curing conditions on the protective performance of an ecofriendly hybrid Si lene sol-gel coating with clay nanoparticles applied on mild steel. *Ind. Eng. Chem. Res.* 53, 10644–10652.
- Beirami, K., Baghshahi, S., Ardestani, M., Riahi, N., 2020. Synthesis and characterization of hydrophobic nano-silica thin coatings for outdoor insulators. *Process. Appl. Ceram.* 14, 40–46.
- Buijnsters, J.G., Zhong, R., Tsyntsaru, N., Celis, J.P., 2013. Surface wettability of macroporous anodized aluminum oxide. *ACS Appl. Mater. Interfaces* 5, 3224–3233.
- Calabrese, L., Capri, A., Fabiano, F., Bonaccorsi, L., Borsellino, C., Proverbio, E., 2015. Corrosion behaviour of a silane protective coating for NdFeB magnets in dentistry, 2015, 345038.
- Cao, R., Zhu, L., Liu, H., Yang, W., Li, W., 2015. The effect of silica sols on electrodeposited zinc coatings for sintered NdFeB. *RSC Adv.* 5, 104375–104385.
- Cao, R., Zhu, L., Liu, H., Li, W., 2017. Electro-deposition and hydrothermal transition of alumina sol film on sintered NdFeB magnets. *Surf. Coat. Technol.* 309, 820–828.
- Chen, J., Xu, B.J., Ling, G.P., 2012. Amorphous Al-Mn coating on NdFeB magnets: electrodeposition from AlCl₃-EMIC-MnCl₂ ionic liquid and its corrosion behavior. *Mater. Chem. Phys.* 134, 1067–1071.
- Chen, J., Xu, J.L., Huang, J., Dai, L., Xue, M.S., Luo, J.M., 2021. Corrosion resistance of T-ZnOw/PDMS-MAO composite coating on the sintered NdFeB magnet. *J. Magn. Mater.* 534.
- Collinson, M.M., 2007. Electrochemistry: an important tool to study and create new sol-gel-derived materials. *Acc. Chem. Res.* 40, 777–783.
- Costenaro, H., Lanzutti, A., Paint, Y., Fedrizzi, L., Terada, M., de Melo, H.G., Olivier, M. G., 2017. Corrosion resistance of 2524 Al alloy anodized in tartaric-sulphuric acid at different voltages and protected with a TEOS-GPTMS hybrid sol-gel coating. *Surf. Coat. Technol.* 324, 438–450.
- Dias, S.A.S., Lamaka, S.V., Diamantino, T.C., Ferreira, M.G.S., 2014. Synergistic protection against corrosion of AA2024-T3 by sol-gel coating modified with La and Mo-enriched zeolites. *J. Electrochem. Soc.* 161, C215–C222.
- Ding, X., Wu, Y., Yang, L., Xu, C., Mao, S., Wang, Y., Zheng, D., Song, Z., 2016. The properties of chromium oxide coatings on NdFeB magnets by magnetron sputtering with ion beam assisted deposition. *Vacuum* 131, 127–134.
- Duan, L.S., Chen, J., Zhang, P.J., Xu, G.Q., Lv, J., Wang, D.M., Shen, W.Q., Wu, Y.C., 2023. Organic-inorganic composite passivation and corrosion resistance of zinc coated NdFeB magnets. *J. Alloy. Compd.* 936.
- Fan, H.-Q., Xia, D.-H., Li, M.-C., Li, Q., 2017. Self-assembled (3-mercaptopropyl) trimethoxysilane film modified with La₂O₃ nanoparticles for brass corrosion protection in NaCl solution. *J. Alloy. Compd.* 702, 60–67.
- Fang, L., He, Q.-Q., Zhou, M.-J., Zhao, J.-P., Hu, J.-M., 2019. Electrochemically assisted deposition of sol-gel films on graphene nanosheets. *Electrochem. Commun.* 109, 106609.
- Fedel, M., Callone, E., Fabbian, M., Deflorian, F., Dirè, S., 2017. Influence of Ce³⁺-doping on molecular organization of Si-based organic/inorganic sol-gel layers for corrosion protection. *Appl. Surf. Sci.* 414, 82–91.
- Foroozan, A., Naderi, R., 2015. Effect of coating composition on the anticorrosion performance of a silane sol-gel layer on mild steel. *RSC Adv.* 5, 106485–106491.
- Gu, Q., Cheng, X., Qi, Y., 2009. Novel self-assembled films of La-based phosphonate 3-aminopropyltriethoxysilane. *J. Rare Earths* 27, 711–716.
- Guin, A.K., Bhadu, M., Sinhababu, M., Mundhara, A., Rout, T.K., Udayabhanu, G., 2014. Effective corrosion inhibition performance of La(NO₃)(3) doped sol-gel coating on galvanized steel sheet. *Anti-Corros. Methods Mater.* 61, 370–379.
- Hamidon, T.S., Hussin, M.H., 2020. Susceptibility of hybrid sol-gel (TEOS-APTES) doped with caffeine as potent corrosion protective coatings for mild steel in 3.5 wt.% NaCl. *Prog. Org. Coat.* 140.
- Kirtay, S., 2014. Preparation of hybrid silica sol-gel coatings on mild steel surfaces and evaluation of their corrosion resistance. *Prog. Org. Coat.* 77, 1861–1866.
- Lakshmi, R.V., Aruna, S.T., 2017. Corrosion protection behaviour of silica-titania hybrid coatings embedded with silica nanoparticles 33, 467–473.
- Latthe, S.S., Hirashima, H., Rao, A.V., 2009. TEOS based water repellent silica films obtained by a co-precursor sol-gel method. *Smart Mater. Struct.* 18.

- Li, Z., Du, Z., Tai, X., Ma, Y., 2021. One-step facile fabrication of hydrophobic SiO₂ coated super-hydrophobic/super-oleophilic mesh via an improved Stober method to efficient oil/water separation. *Colloids Surf. A – Physicochem. Eng. Aspects* 623.
- Li, X., Li, J., Xu, K., Wang, Z., Bian, Y., Shao, Y., Hu, C., Ni, J., 2022. Effect of nano-TiC dopant size on magnetic properties and corrosion resistance of hot-deformed NdFeB. *J. Rare Earths* 40, 930–936.
- Li, J., Mao, S., Sun, K., Li, X., Song, Z., 2009. AlN/Al dual protective coatings on NdFeB by DC magnetron sputtering. *J. Magn. Magn. Mater.* 321, 3799–3803.
- Liu, D., Zhao, W., Liu, S., Cen, Q., Xue, Q., 2016. Comparative tribological and corrosion resistance properties of epoxy composite coatings reinforced with functionalized fullerene C60 and graphene. *Surf. Coat. Technol.* 286, 354–364.
- Metroke, T., Wang, Y., van Ooij, W.J., Schaefer, D.W., 2009. Chemistry of mixtures of bis-[trimethoxysilylpropyl]amine and vinyltriethoxysilane: an NMR analysis. *J. Sol-Gel Sci. Technol.* 51, 23–31.
- Motte, C., Poelman, M., Roobroeck, A., Fedel, M., Deflorian, F., Olivier, M.G., 2012. Improvement of corrosion protection offered to galvanized steel by incorporation of lanthanide modified nanoclays in silane layer. *Prog. Org. Coat.* 74, 326–333.
- Nakajima, A., 2011. Design of hydrophobic surfaces for liquid droplet control. *NPG Asia Mater.* 3, 49–56.
- Olivieri, F., Castaldo, R., Cocca, M., Gentile, G., Lavorgna, M., 2021. Mesoporous silica nanoparticles as carriers of active agents for smart anticorrosive organic coatings: a critical review. *Nanoscale* 13, 9091–9111.
- Ouyang, Y., Qiu, R., Xiao, Y., Shi, Z., Hu, S., Zhang, Y., Chen, M., Wang, P., 2019. Magnetic fluid based on mussel inspired chemistry as corrosion-resistant coating of NdFeB magnetic material. *Chem. Eng. J.* 368, 331–339.
- Parhizkar, N., Ramezanzadeh, B., Shahrabi, T., 2017. Enhancement of the corrosion protection properties of a hybrid sol-gel based silane film through impregnation of functionalized graphene oxide nanosheets. *J. Electrochem. Soc.* 164, C1044–C1058.
- Pourhashem, S., Rashidi, A., Vaezi, M.R., Bagherzadeh, M.R., 2017. Excellent corrosion protection performance of epoxy composite coatings filled with amino-silane functionalized graphene oxide. *Surf. Coat. Technol.* 317, 1–9.
- Purcar, V., Raditoiu, V., Dumitru, A., Nicolae, C.-A., Frone, A.N., Anastasescu, M., Raditoiu, A., Raduly, M.F., Gabor, R.A., Caprarescu, S., 2019. Antireflective coating based on TiO₂ nanoparticles modified with coupling agents via acid-catalyzed sol-gel method. *Appl. Surf. Sci.* 487, 819–824.
- Qiao, Y., Li, W., Wang, G., Zhang, X., 2015. Corrosion protection of AZ31 magnesium alloy treated with La³⁺ modified 3-methacryloxypropyltrimethoxysilane conversion film. *J. Rare Earths* 33, 647–654.
- Ramezanzadeh, B., Raeisi, E., Mahdavian, M., 2015. Studying various mixtures of 3-aminopropyltriethoxysilane (APS) and tetraethylorthosilicate (TEOS) silanes on the corrosion resistance of mild steel and adhesion properties of epoxy coating. *Int. J. Adhes. Adhes.* 63, 166–176.
- Rodošek, M., Kreta, A., Gabersček, M., Šurca Vuk, A., 2024. Ex situ IR reflection-absorption and in situ AFM electrochemical characterisation of the 1,2-bis(trimethoxysilyl)ethane-based protective coating on AA 2024 alloy. *Corros. Sci.* 102 (2016), 186–199.
- Saji, V.S., 2019. Review of rare-earth-based conversion coatings for magnesium and its alloys. *J. Mater. Res. Technol.-Jmr&t* 8, 5012–5035.
- Santana, I., Pepe, A., Schreiner, W., Pellice, S., Cere, S., 2016. Hybrid sol-gel coatings containing clay nanoparticles for corrosion protection of mild steel. *Electrochim. Acta* 203, 396–403.
- Shen, L., Wang, Y., Jiang, W., Liu, X., Wang, C., Tian, Z., 2017. Jet electrodeposition multilayer nickel on the surface of sintered NdFeB and corrosion behaviours. *Corros. Eng. Sci. Technol.* 52, 311–316.
- Sheridan, R.S., Williams, A.J., Harris, I.R., Walton, A., 2014. Improved HDDR processing route for production of anisotropic powder from sintered NdFeB type magnets. *J. Magn. Magn. Mater.* 350, 114–118.
- Song, T.T., Tang, X., Yin, W.Z., Ju, J.Y., Wang, Z.X., Liu, Q.B., Tang, Y., Chen, R.J., Yan, A.R., 2019. Magnetic properties improvement of hot-deformed Nd-Fe-B permanent magnets by Pr-Cu eutectic pre-diffusion process. *Acta Mater.* 174, 332–341.
- Taheri, M., Naderi, R., Saremi, M., Mahdavian, M., 2017. Development of an ecofriendly silane sol-gel coating with zinc acetylacetonate corrosion inhibitor for active protection of mild steel in sodium chloride solution. *J. Sol-Gel Sci. Technol.* 81, 154–166.
- Tang, J., Yao, Y., Guo, M., Jiang, J., Cong, H., Chen, Y., Sun, Y., Kong, Y., Han, S., 2021. Anticorrosion and repair behavior of rec-SiO₂ silane film on carbon steel, 28, 2150098.
- Telmenbayar, L., Ramu, A.G., Erdenebat, T.-O., Choi, D., 2022. Anticorrosive lanthanum embedded PEO/GPTMS coating on magnesium alloy by plasma electrolytic oxidation with silanization. *Mater. Today Commun.* 33.
- Toorani, M., Aliofkhaezai, M., Golabadi, M., Rouhaghdam, A.S., 2017. Effect of lanthanum nitrate on the microstructure and electrochemical behavior of PEO coatings on AZ31 Mg alloy. *J. Alloy. Compd.* 719, 242–255.
- Vennerberg, D., Rueger, Z., Kessler, M.R., 2014. Effect of silane structure on the properties of silanized multiwalled carbon nanotube-epoxy nanocomposites. *Polymer* 55, 1854–1865.
- Wu, Y., Gao, Z., Xu, G., Liu, J., Xuan, H., Liu, Y., Yi, X., Chen, J., Han, P., 2021. Current status and challenges in corrosion and protection strategies for sintered NdFeB magnets. *Acta Metall. Sin.* 57, 171–181.
- Wu, L.-K., Liu, L., Li, J., Hu, J.-M., Zhang, J.-Q., Cao, C.-N., 2010. Electrodeposition of cerium (III)-modified bis-[triethoxysilylpropyl]tetra-sulphide films on AA2024-T3 (aluminum alloy) for corrosion protection. *Surf. Coat. Technol.* 204, 3920–3926.
- Wu, L.-K., Hu, J.-M., Zhang, J.-Q., Cao, C.-N., 2013. Superhydrophobic surface constructed on electrodeposited sol-gel silica film. *Electrochem. Commun.* 26, 85–88.
- Xu, F.-F., Zhao, Y., Xu, Y., 2023. Preparation and corrosion resistance of rare earth-silane composite conversion coatings on magnesium-lithium alloy surface. *Rare Met.* 42, 1011–1017.
- Xue, B., Yu, M., Liu, J., Liu, J., Li, S., Xiong, L., 2017. Corrosion protection of AA2024-T3 by sol-gel film modified with graphene oxide. *J. Alloy. Compd.* 725, 84–95.
- Yang, H., Mao, S., Song, Z., 2012. The effect of absorbed hydrogen on the corrosion behavior of sintered NdFeB magnet. *Mater. Corros.-Werkstoffe Korrosion* 63, 292–296.
- Yang, H., Duan, L., Zhang, P., Xu, G., Cui, J., Lv, J., Sun, W., Li, B., Wang, D., Wu, Y., 2022. Corrosion resistance of functionalized carbon nanotubes enhanced epoxy coatings on sintered NdFeB magnets. *J. Coat. Technol. Res.* 19, 1317–1329.
- Yang, C., Xu, W., Meng, X., Shi, X., Shao, L., Zeng, X., Yang, Z., Li, S., Liu, Y., Xia, X., 2021. A pH-responsive hydrophilic controlled release system based on ZIF-8 for self-healing anticorrosion application. *Chem. Eng. J.* 415, 128985.
- Zand, R.Z., Flexer, V., De Keersmaecker, M., Verbeke, K., Adriaens, A., 2016. Self-healing silane coatings of cerium salt activated nanoparticles. *Mater. Corrosion-Werkstoffe Korrosion* 67, 693–701.
- Zhang, K., Wang, Z., He, J., Li, X., Gong, W., Huang, Y., 2022. Coupling effects of hydrogen and Dy/Nb on magnetic properties of sintered NdFeB magnets. *Int. J. Hydrogen Energy* 47, 14027–14038.
- Zhang, H., Yin, L., Shi, S., Liu, X., Wang, Y., Wang, F., 2015. Facile and fast fabrication method for mechanically robust superhydrophobic surface on aluminum foil. *Microelectron. Eng.* 141, 238–242.
- Zhang, H.H., Zhang, X., Bian, H., Zhang, L., Chen, Y., Yang, Y., Zhang, Z., 2024. Benzotriazole loaded CeO₂ nano-containers towards superior anti-corrosive silane coating for protection of copper. *Colloids Surf. A Physicochem. Eng. Asp.* 682, 132844.
- Zhang, P., Zhu, M., Li, W., Xu, G., Huang, X., Yi, X., Chen, J., Wu, Y., 2018. Study on preparation and properties of CeO₂/epoxy resin composite coating on sintered NdFeB magnet. *J. Rare Earths* 36, 544–551.
- Zhang, P., Liu, Q., Huang, J., Cui, J., Sun, W., Li, B., Xu, G., 2022. Phosphate conversion of electroplated Ni coatings on NdFeB magnets improving the anticorrosion property. *J. Alloy. Compd.* 922.
- Zheng, J., Lin, M., Xia, Q., 2012. A preparation method and effects of Al-Cr coating on NdFeB sintered magnets. *J. Magn. Magn. Mater.* 324, 3966–3969.
- Zhong, F., He, Y., Wang, P., Chen, C., Xie, P., Li, H., Chen, J., 2019. One-step hydrothermal synthesis of reduced graphene oxide/aspartic acid intercalated layered double hydroxide for enhancing barrier and self-healing properties of epoxy coating. *React. Funct. Polym.* 145, 104380.